Reducing Inverter Losses by Obtaining Optimal Switching Frequency in IPMSM Drives

Osman Emre Özçiflikçi
Electrical-Electronic Engineering
Kirsehir Ahi Evran University
Kirsehir/Turkey
osman.ozciflikci@ahievran.edu.tr

Mikail Koç
Electrical-Electronic Engineering
Kirsehir Ahi Evran University
Kirsehir/Turkey
mkoc@ahievran.edu.tr

Serkan Bahçeci
Electrical-Electronic Engineering
Erciyes University
Kayseri/Turkey
sbahceci@erciyes.edu.tr

2024 6th Global Power, Energy and Communication Conference (GPECOM) | 979-8-3503-5108-8/24/$31.00 ©2024 IEEE | DOI: 10.1109/GPECOM61896.2024.10582581

***Abstract*— Interior mounted permanent magnet synchronous machines (IPMSMs), which seem to be more attractive among electric machines in terms of high efficiency and high power/torque densities, are widely used in the industry. Therefore, IPMSM design and their drives are popular topics in both academia and industry. In this study, the trade-off between IGBT driver losses and current quality has been investigated by obtaining the optimal switching frequency applying the Field-Oriented Control (FOC) technique, which is widely used in IPMSM drives. In experimental studies, current waveforms have been compared at switching frequencies of about 1.5, ~5, 12, and 15 times the maximum electrical frequency of a 4.1kW prototype machine under study. It has been validated that the current harmonics increase with reduced switching frequency, while the inverter losses increase and become more severe with increased switching frequency. While the improvement in the current waveforms with increasing switching frequency is significant to some extent, the improvement become relatively low with further increased switching frequency where inverter losses become more severe. Thus, the optimal switching frequency can be obtained based on the trade-off between the current quality and the inverter losses.**

Keywords—IPMSM, optimal switching frequency, maximum machine speed, inverter losses

I. INTRODUCTION

Permanent magnet synchronous machines (PMSMs) are frequently used in industrial applications such as electric vehicles [1], electric aircraft [2], elevator traction system [3] due to their superior features such as high efficiency, low acoustic noise, and high power/torque density. PMSMs are classified into two categories as surface-mounted PMSM (SPMSM) and interior-mounted PMSM (IPMSM), depending on the placement of the magnets on the rotor [4]. While SPMSMs only produce torque depending on the magnet flux linkage, IPMSMs have the potential to produce reluctance torque in addition to magnet-induced torque, since the -dq axis inductances are different from each other. Hence, IPMSMs may be seen as more advantageous in applications where high torque density is required. However, the fact that IPMSMs produce both magnet and reluctance torque, this brings control complexity in terms of obtaining maximum torque with minimum stator current. Unlike SPMSMs, because torque production does not depend solely on the magnet flux linkage and -q axis current in IPMSMs, maximum torque per ampere (MTPA) strategies must be applied [5, 6]. Since the MTPA strategy includes complex operations such as mathematical analysis, signal injection methods, and search algorithms [7, 8] the control of IPMSMs seems to be more complex than SPMSMs.

Field-Oriented Control (FOC) is a vector control technique and it is widely used in the control of PMSMs [9-11]. It works on the principle of transforming the 3-phase currents into -dq axis currents and regulating them by comparing with the command -dq axis currents, where the errors are driven to zero with PI regulators. Although the direct torque control (DTC) technique is widely used in PMSM control in the literature [12-14], the accuracy of the flux and torque observer used in DTC drives is of vital importance for the drive. Considering that the parameters variation in the flux and torque observers, the DTC strategy may have lower performance compared to the FOC technique. In addition, when the FOC technique is used for control of IPMSMs, the technique may be more advantageous since the current limits can directly be posed in the drive. For this reason, the FOC technique has been adopted in the IPMSM drive in this study.

Whether SPMSM or IPMSM is employed in a drive, the pulse width modulation (PWM) technique plays an important role on the behavior of the drive. Since the adopted PWM strategy to drive an AC machine directly affect 3-phase current distortions, total harmonic distortions (THD) of phase currents, undesired torque ripples, and DC bus voltage utilization ratio, a care should be taken in choosing the PWM strategy. In the literature, sinusoidal PWM (SPWM), third harmonic injected PWM (THIPWM) and space vector PWM (SVPWM) strategies are commonly used modulation strategies for inverters [15]. Compared to SPWM and THIPWM strategies, SVPWM strategy has wide use in power converters due to its superior features such as lower current harmonics, lower switching losses, and higher DC bus voltage utilization ratio [16]. Although it is possible to reduce current harmonics and torque ripple ratio by developing PWM strategies in machine drives, correctly determining the inverter switching frequency for each PWM strategies is also effective on distortions. Since high and low switching frequencies increase inverter losses and current harmonics, respectively, the drives need to be operated at the optimal switching frequency.

Since the use of power converters is a must to drive AC machines in real life experiments, it is important to develop control algorithms to reduce power electronics based performance degradation. Modulation strategies can be classified into two categories based on the switching frequency. Whether the machine is driven by FOC or DTC strategy, the modern AC drives can have either constant or variable switching frequency. It is undesirable that the switching frequency is not constant in the hysteresis-based DTC control technique and model predictive control technique as they have variable switching frequency. Therefore, space vector DTC technique [17, 18] and modulated MPC techniques [19, 20] have been developed to ensure a constant switching frequency. Variable switching frequency has a negative influence on 3-phase current distortions and total harmonic distortion (THD), and thus on torque ripples. In applications where a fixed switching frequency is used, 3-phase current distortions and THD can be optimized by determining the switching frequency appropriately.

979-8-3503-5108-8/24/$31.00 ©2024 IEEE

From this perspective, the behavior of the drive has been analyzed in this study by altering the switching frequency on the FOC-based IPMSM drive, provided that all other conditions were the same. In addition, the variation of losses with varying switching frequency and the distortions in 3-phase currents have been compared and the optimal switching frequency is obtained considering the maximum speed of the machine. In this study, an IPMSM drive operating with a fixed switching frequency has been designed and different switching frequencies have been tested in the FOC-based drive and the results have been monitored. The aim of the study is to experimentally monitor switching frequency, 3-phase current distortions, THD and losses in the IGBT drives and to determine how to select the optimal switching frequency considering the maximum electrical frequency of the motor.

II. Mathematical Expressions

IPMSM on the -dq axis can be modeled as in (1-3) with Clark and Park transformations [5]. The peak convention is adopted, and the rotating -dq axis control frame is illustrated in Fig. 1.

$$\begin{bmatrix} V_d \\ V_q \end{bmatrix} = R\begin{bmatrix} I_d \\ I_q \end{bmatrix} + \frac{d}{dt}\begin{bmatrix} \Psi_d \\ \Psi_q \end{bmatrix} + \omega\begin{bmatrix} -\Psi_q \\ \Psi_d \end{bmatrix} \quad (1)$$

$$\begin{bmatrix} \Psi_d \\ \Psi_q \end{bmatrix} = \begin{bmatrix} L_d & 0 \\ 0 & L_q \end{bmatrix}\begin{bmatrix} I_d \\ I_q \end{bmatrix} + \begin{bmatrix} \Psi_m \\ 0 \end{bmatrix} \quad (2)$$

$$T_e = \frac{3p}{2}\left(\Psi_m I_q - I_d I_q\left(L_q - L_d\right)\right) \quad (3)$$

V_d,V_q are voltage amplitudes (Volt) and I_d, I_q are current amplitudes (Ampere) in -dq frame, ω_e and ω_m are the electrical and mechanical speed in rad/s, respectively, p is the pole-pair number, L_d and L_q are the inductance values (Henry) of -d and -q axis, respectively, Ψ_m is the permanent magnet flux linkage (Weber) and R_s is the stator resistance (ohm). T_e is the electromagnetic torque in Nm. Ψ_d,Ψ_q are flux amplitudes (Weber) in –dq frame.

As can be seen from Fig. 2, the commands of the system are stator current amplitude and current angle β. 3 phase currents measured from the machine are transformed into the -dq axis with Clark and Park transformations. Then, by comparing the command and measured -dq axis currents, the resulting errors are driven to zero with the help of PI regulators. The produced -dq axis voltage values are fed to the over modulation block to adopt the voltage limits according to the modulation strategy of the drive. Since the SVPWM strategy has been used in this study, the voltage amplitude has been limited to $V_{DC}/\sqrt{3}$.

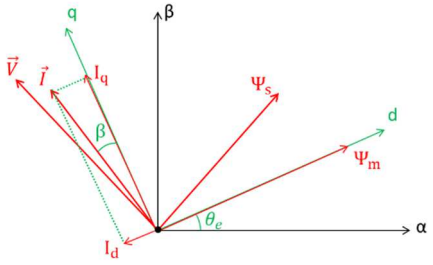

Fig. 1. Stationary and rotating frames

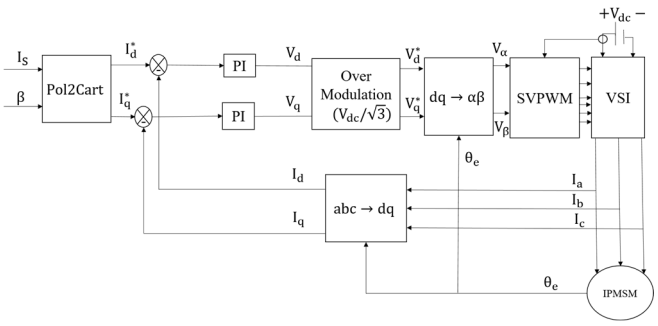

Fig. 2. IPMSM drive schematic

A. MTPA Strategy

IPMSMs have the potential to produce reluctance torque due to the difference in -dq axis inductances as it is well known as saliency ratio. This shows the superiority of IPMSMs over other machines due to their higher torque production capability. However, it can be deduced from (3) that the MTPA strategy must be applied in order to use the potential of producing reluctance torque. Therefore, in this study, the MTPA current angle corresponding to given stator current amplitudes have been determined through numerical solutions and reluctance torque production has been utilized to achieve high efficiency operation. The drive is operated by producing command -dq axis currents where the electromagnetic torque production is maximized with minimum stator current amplitude. Utilizing (4-5) and by equalizing the derivative of torque in (3) with respect to β current angle shown in Fig.1 to zero, the optimum current commands are obtained. It should be noted that recent studies to improve the accuracy of numerical solutions for MTPA operation further discusses the optimum trajectory in practical IPMSM drives [7,8].

$$\begin{bmatrix} I_d \\ I_q \end{bmatrix} = I_s * \begin{bmatrix} -\sin\beta \\ \cos\beta \end{bmatrix} \quad (4)$$

$$|I_s| = \sqrt{{I_d}^2 + {I_q}^2} \quad (5)$$

where I_s is stator current amplitude and β is stator current angle in Fig. 1.

B. Determination of Control Parameters

The parameters of PI regulators can be tuned based on the desired cut-off frequency of the system, as stated in [21]. The system is operated by determining the switching frequency in the SVPWM block. In Clark and Park transformations, the system must be implemented considering whether it is aligned to phase A or 90 degrees behind phase A. Otherwise, the drive cannot perform the control process and the system will not achieve stable operation. Therefore, transformation conventions must be determined carefully when converting both SVPWM and 3-phase currents to -dq axis currents or voltages. This paper adopts peak convention in -dq frames shown in Fig. 1.

III. Experimental Results

Fig. 3 shows the test setup created to drive the prototype IPMSM machine. The DC power supply, which is connected to the grid, has a DC output voltage of 0-1500 V and an output power capacity of 15 kW. The DC power supply is connected to a commercial inverter with a DC bus maximum voltage of 1100 V and a maximum AC output voltage of 530 V. The characteristics of the IPMSM to be tested are given in Table I.

According to Table I, DC power supply is used in the machine drive system by setting it at 120 V level.

The dSpace-RTI 1202 MLBX controller is employed to control the machine drive system. The signal outputs received from the dSpace controller are at 5 V level. However, the inverter works with signals at 24 V level. An optocoupler circuit has been designed and employed to provide isolation between the controller and the inverter and to feed the inverter by pulling the 5 V level signal up to 24 V level. In addition, the auxiliary power supply is supported by a UPS connection to prevent the inverter from experiencing a momentary outage against the risk of power failure.

Dyno is employed for keeping the speed at the desired level during current and torque control. Based on the data catalogue of the dynamometer, the speed can be controlled by applying a current-controlled load with a power supply to determine the brake level. Hence, dyno controller is operated as voltage controlled current source in the drive system. In addition, the torque transducer is also used in the drive system for the measurement of actual torque. The nominal torque measurement value of the torque transducer is 20 Nm. As can be seen in Table I, the employed torque transducer is suitable for the test system considering the continuous torque value of the machine.

Since the control algorithm used in experimental studies is FOC, rotor position information is needed when performing Clarke and Park transformations. Therefore, absolute encoder is employed for position measurement. Since the control is achieved in rotating rotor reference frame, the accurate rotor position angle is vital and hence the accurate calibration of initial rotor position angle is a must. The initial mechanical rotor position angle has been obtained as 60° in the test rig. In addition, the ABC-phase currents have been measured by current transducers at the output of the inverter. The current probe shown in Fig. 3 is employed for calibration of phase current measurements. The gain of current transducers have been obtained as 21,87 $mV.A^{-1}$ scaling factor in the experiments. Thus, closed loop control is achieved by accurate measurements of feedback variables.

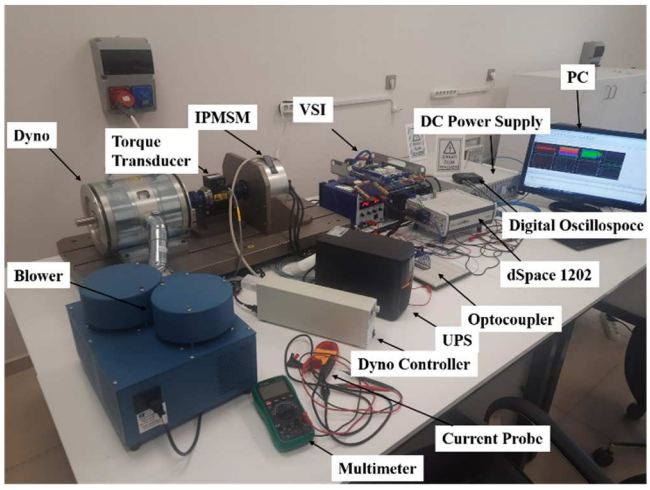

Fig. 3. Test setup

As can be seen in Fig. 4, the drive has been operated by setting the command stator current amplitude to 30 A and the MTPA current angle β is 28.92°. In Fig. 4, the filtered form of the electromagnetic torque produced by the machine, waveforms of 3 phase currents, SVPWM duty cycle S_{abc}, mechanical speed ω_m, reference and actual values of –dq axis currents and stator current amplitude are given. The measured torque value has been filtered deliberately for clear illustration. It is aimed to compare the distortions in 3-phase currents by obtaining these test results for given switching frequency values to be tested. In addition, the duty cycle values produced by SVPWM are as given in Fig. 4 for 8 kHz switching. Accordingly, distortions in the drive can be compared against switching frequencies via duty cycle.

TABLE I. Parameters of IPMSM

Type	IPMSM
Number of phase	3
Number of pole pairs	4
Continuous Torque	15.7 Nm
Continuous Power	4.1 kW
-dq Axis Inductances	L_d = 0.282 mH, L_q =0.828 mH
Flux Linkage	Ψ_m = 0.0182 Wb
Stator Resistance	R_s = 0.0463 Ω
Inertia	J=0.0071572 kg*m^2
Input Voltage Range	12 V – 600 V
Maximum Speed	10000 rpm

It should be noted that the drive operating conditions, the command stator current amplitudes, and the optimum current angle commands are all the same in each drive under comparison except the switching frequencies. In addition, the speed of the machine needs to be same at all switching frequencies for fair comparisons. Since the machine is controlled under torque control mode and the dyno is a passive load, the machine speed is not precisely controlled, and the test results have been obtained while the machine operates around 1000 rpm as in Fig. 4.

Considering that the maximum speed of the prototype IPMSM is 10 krpm, it can be obtained from (6) and (7) that the machine under study will have a maximum mechanical and electrical frequencies of 166.67 Hz and 666.67 Hz, respectively, since it is an 8-pole machine.

$$f_{max\_mech} = \text{Max. mech. Speed} / 60 \quad (6)$$

$$f_{max\_elect} = p * f_{max\_mech} \quad (7)$$

Since the maximum electrical frequency of the machine is 666.67 Hz, the comparisons have been made by selecting switching frequencies of 1 kHz, 3.5 kHz, 8 kHz and 10 kHz, which are 1.5, ~5, 12 and 15 times the maximum electrical frequency of the machine, respectively. It is important to note that since sampling error and stability issues will arise at low sampling to operating frequency ratio [22], the lowest switching frequency has been selected as 1.5 times the maximum operating frequency in the case study.

Fig. 5 compares the 3-phase current waveforms measured from the inverter output at different switching frequencies. As can be clearly seen from Fig. 5, current harmonics at the 1 kHz switching frequency are considerably higher than other switching frequencies. It can be observed that the distortions from the 3-phase current waveforms are relatively close to

each other at the switching frequencies of 3.5 kHz, 8 kHz and 10 kHz.

The reason for making comparisons on 3-phase current waveforms is because current distortions directly affect torque ripple. In other words, it can be said that the torque ripple ratio of the drive with 1 kHz switching frequency, is higher than the others since its 3-phase current waveforms has more distortion. High 3-phase current distortions and torque ripples results in deteriorated operation of the machine in terms of acoustic noise, higher temperature, increased machine losses and reduced operating life as the torque quality decreases. On the other hand, inverter losses will increase when operating the machine with higher switching frequencies.

The stator current amplitudes measured from the drives are compared in Fig. 6 in order to illustrate the influence of the total harmonic distortions (THD) on the current waveforms. Accordingly, it is seen that the current ripple ratio and therefore the torque ripple ratio of the drive operated with 1 kHz switching frequency is quite high compared to the others. In addition, Fig. 7 proves that the THD ratios of drives operated with 3.5, 8 and 10 kHz switching frequencies are relatively close to each other as has been discussed in Fig. 5.

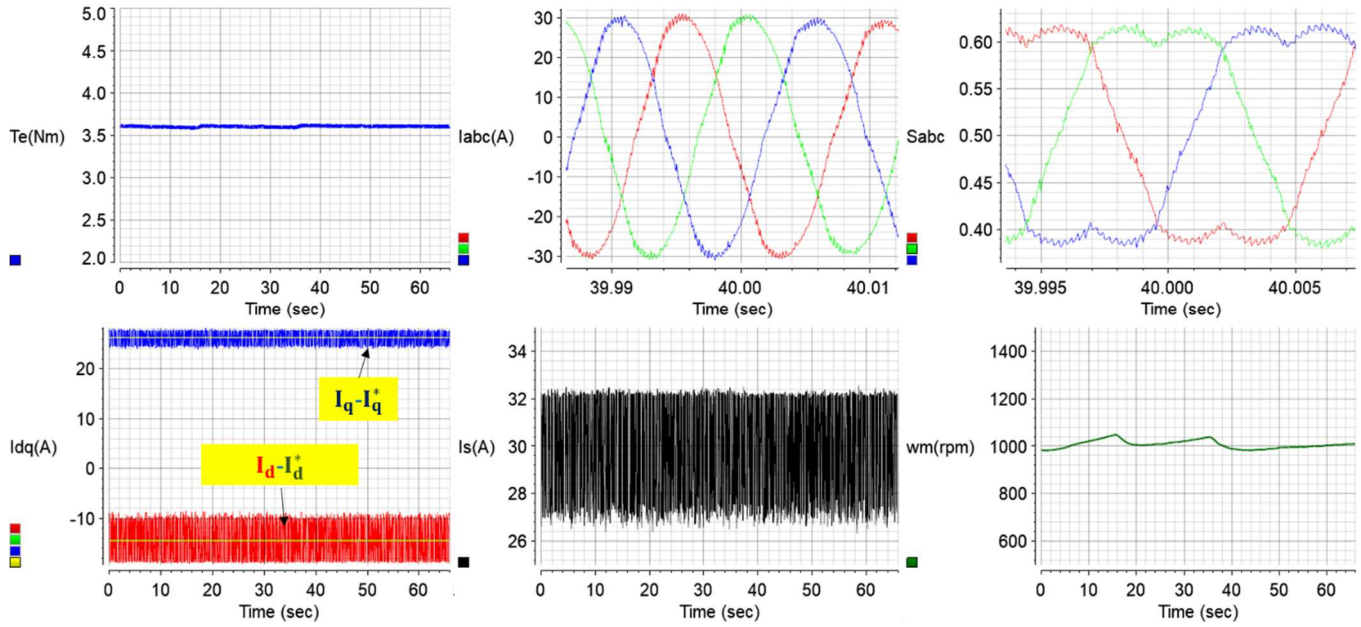

Fig. 4. Drive results under 8 kHz switching frequency

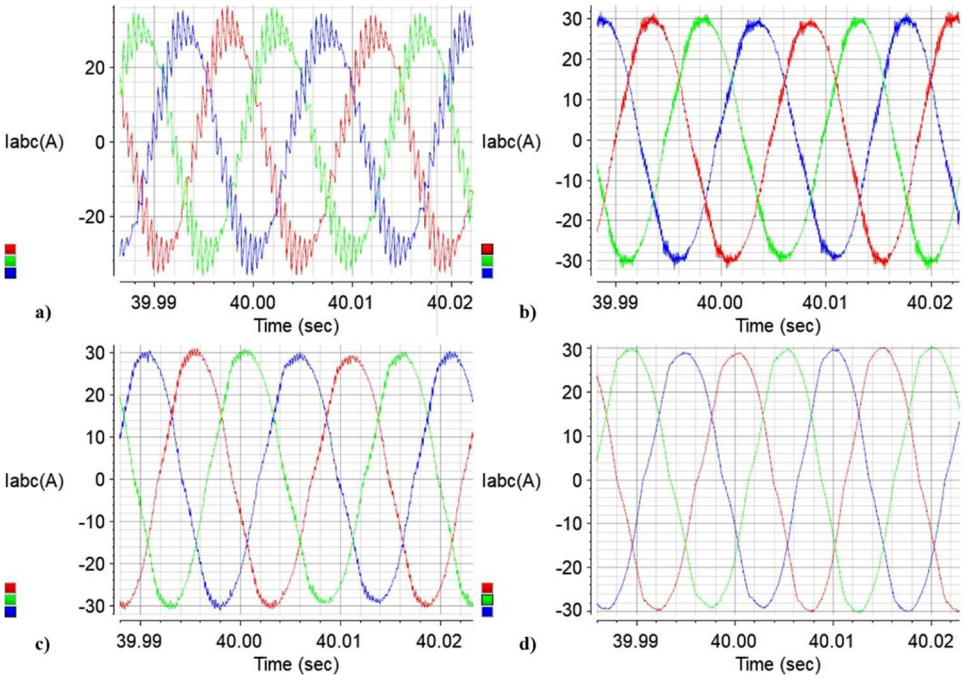

Fig. 5. Comparison of current waveforms at different switching frequencies.a) 1 kHz, b) 3.5 kHz, c) 8 kHz, d) 10 kHz

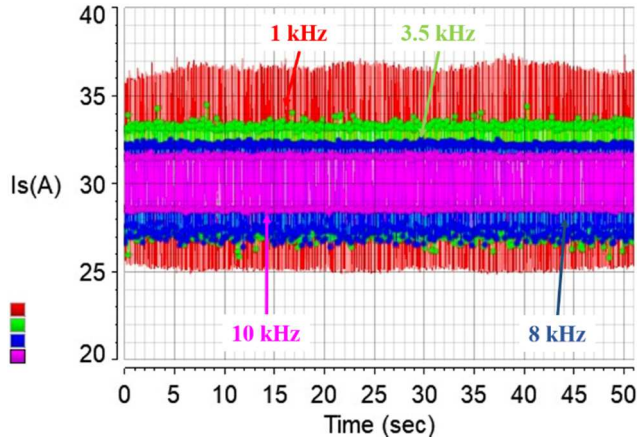

Fig. 6. Comparison of stator current amplitudes

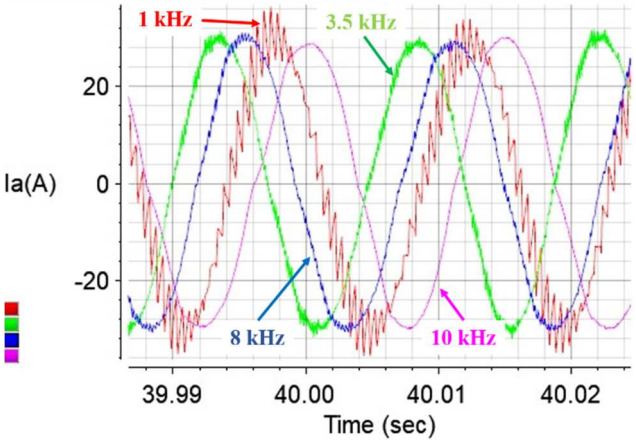

Fig. 7. Comparison of phase A currents

Fig. 7 shows the comparison of phase-A currents from which THD measurements have been obtained. In Fig. 7, it is aimed to determine the effect of switching frequency on current ripple by zooming in the peaks of phase-A currents. As can be seen, at lower switching frequency such as 1 kHz, the ripple increases and acoustic noise issue much arises. It should be noted that the phase difference is because the tests have been done separately for each sampling period. Fig. 8 compares the THD ratios of the drive operated with 4 different switching frequencies. Based on the results, it is clear that the current and torque quality of the drive operating at low switching frequencies will be much deteriorated whereas the improvement with the increased switching frequencies will be marginal after some extent.

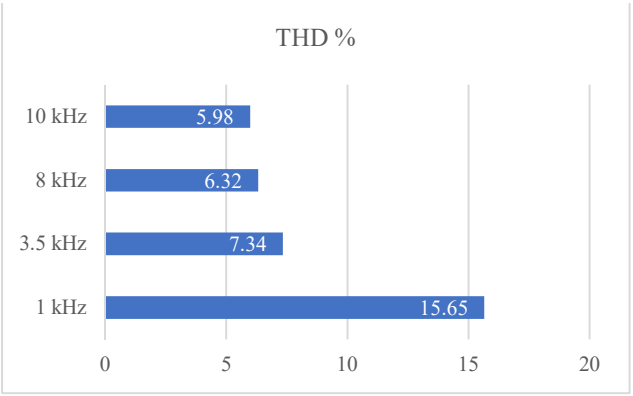

Fig. 8. Comparison of Total Harmonic Distortion Percentage

Since the voltage drop on the active semiconductor devices and their equivalent on state resistances are nonlinear and highly depends on the operating torque (current) and temperature, inverter losses can only be estimated. Rather, since the power consumed by inverter control circuit can be measured and there is direct proportion between the two powers, the power consumed by IGBT drivers has been obtained. The auxiliary power source that feeds the power electronics circuit used in the test system is employed as a constant 24 V voltage source. While the voltage applied to the inverter control circuit is constant at 24 V, the DC current values supplied to the power electronics circuit is different at different switching frequencies. The current amplitudes have been monitored and recorded for each experiment. As can be seen in Fig. 9, the current drawn into the inverter control circuit is lower at low switching frequency, while the current increases as the switching frequency increases. The drives operate at 1 kHz, 3.5 kHz, 8 kHz, and 10 kHz switching frequencies draw 340, 370, 420 and 450 mA, respectively. When calculation is made for power loss in the power electronics circuit, the power consumed by the inverter at 1 kHz switching frequency is obtained as 8.16 W, while it is observed that 10.8 W power is consumed at 10 kHz switching frequency. The power difference between the two switching frequencies in experimental studies is obtained as 1.84 W. Hence, the results validate that the optimum switching frequency is obtained based on the trade-off between the THD improvement and the system losses. Recording the current values drawn by the inverter control circuit during experimental studies does not directly represent inverter losses. However, it is included in the study as an indicator that inverter losses increase with increasing switching frequency. It can be stated that by increasing the switching frequency, undesired and indispensable voltage drop based losses on active switch and the freewheeling diodes will also increase. The purpose of this study is to determine at what level the switching frequencies of IPMSM drives can be optimized considering the trade-off between the losses and the torque quality.

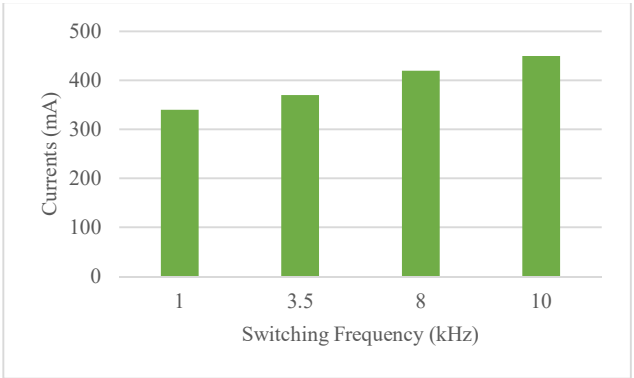

Fig. 9. Inverter Control Circuit Currents

Optimizing IPMSM drives considering current harmonics, THD and inverter losses is very important for drive performance. Because reducing current distortions and THD percentages will increase the torque quality and the operation life of the machine at long term. On the other hand, reducing inverter losses also makes the drive more efficient. It is well known that the efficiency improvement facilitates more compact design of the components. Based on these research results, it is predicted that new

researchers working on IPMSM drives can choose a switching frequency according to the maximum electrical frequency of IPMSM.

IV. Conclusion

In this study, experimental studies have been carried out on the IPMSM drive, which is a type of PMSM that is widely used in the industry due to its superior features such as high efficiency, high torque/power density and low acoustic noise. The drive has been implemented by applying the FOC technique, which is widely used in IPMSM drives. It is aimed to monitor 3-phase current waveforms, THD ratios, and losses in the IGBT drives by varying the switching frequencies in the SVPWM strategy. Although a decrease in the phase current distortions is observed by increasing the switching frequency, it has been seen that determining the switching frequency above ~10 times the maximum electrical frequency of the machine increases the losses on the power electronics circuit while the improvement of the current quality is marginal. Adjusting the switching frequency at a low level, around 1.5 and ~5 times the maximum electrical frequency of the machine, much increase the 3-phase current distortions. Also, audible noise issue appears at lower sampling periods. Hence, inverter switching frequency can be optimized based on the trade-off between actuator losses and current quality. The findings offer novel approaches to obtain online optimization strategies of sampling periods for power converters based on the machine operation speed. This is because the trade-off discussed above can be optimized for varying speeds of the machine. Hence, the optimization can be further improved for wide range operation.

Acknowledgment

This study has been supported by the Scientific and Technological Research Council of Turkey (TUBITAK) through the Scientific and Technological Research Projects Funding Program (1001) with a project numbered as 118E858

References

[1] D. Zhou, K. Luo, Z. Shen, and J. Zou, "Vector-Space-Decomposition-Based Power Flow Control of Single-Stage-Multiport-Inverter-Fed PMSM Drive for Hybrid Electric Vehicles," *IEEE Transactions on Industrial Electronics,* pp. 1-11, 2023.

[2] Y. Wang, S. Fang, J. Hu, and D. Huang, "A Novel Active Disturbance Rejection Control of PMSM Based on Deep Reinforcement Learning for More Electric Aircraft," *IEEE Transactions on Energy Conversion,* vol. 38, pp. 1461-1470, 2023.

[3] D. Niu and D. Song, "Model-Based Robust Fault Diagnosis of Incipient ITSC for PMSM in Elevator Traction System," *IEEE Transactions on Instrumentation and Measurement,* vol. 72, pp. 1-12, 2023.

[4] X. Zhang, C. Zhang, Z. Wang, and J. Rodríguez, "Motor-Parameter-Free Model Predictive Current Control for PMSM Drives," *IEEE Transactions on Industrial Electronics,* pp. 1-10, 2023.

[5] O.E. Özçiflikçi, M. Koç, S. Bahçeci, "Maximum Torque per Ampere Strategy in IPM Drives for Electric Vehicles," *El-Cezeri,* vol. 8, pp. 1405-1415, September. 2021.

[6] C. Lee and I. G. Jang, "Topology Optimization of the IPMSMs Considering Both the MTPA and FW Controls Under the Voltage and Current Limitations," *IEEE Transactions on Industrial Electronics,* vol. 70, pp. 8244-8253, 2023.

[7] K. Li, T. Sun, J. Liang, M. Koc, and Y. Zhou, "Automatic MTPA Control for IPMSM Drives Based on Pseudorandomly Reversed Fixed-Frequency Sinusoidal Signal Injection," *IEEE Transactions on Industrial Electronics,* pp. 1-12, 2023.

[8] Z. H. Qiu and Y. S. Lai, "New On-line MTPA Angle Search and Control Methods Based on Digital Twins for IPM Synchronous Motor Drives Considering Motor Non-linearity," *IEEE Access,* pp. 1-1, 2023.

[9] J. Xu, Z. Wei, and S. Wang, "Active Disturbance Rejection Repetitive Control for Current Harmonic Suppression of PMSM," *IEEE Transactions on Power Electronics,* vol. 38, pp. 14423-14437, 2023.

[10] S. Zhou, Z. Zhang, H. Li, Z. Li, Q. Xing, X. Liu*, et al.*, "A Robust Encoderless Control for PMSM Drives: A Revised Hybrid Active Flux-Based Technique," *IEEE Transactions on Power Electronics,* vol. 38, pp. 14438-14449, 2023.

[11] S. S. Kuruppu, S. G. Abeyratne, and S. Hettiarachchi, "Modeling and Detection of Dynamic Position Sensor Offset Error in PMSM Drives," *IEEE Access,* vol. 11, pp. 36741-36752, 2023.

[12] Y. Liu, M. Lyu, S. Huang, W. Liao, G. Liang, C. Feng*, et al.*, "Direct Torque Control Schemes for Dual Three-Phase PMSM Considering Unbalanced DC-link Voltages," *IEEE Transactions on Energy Conversion,* pp. 1-14, 2023.

[13] W. Deng, X. Zhang, and B. Yan, "An Enhanced Discrete Virtual Vector- Based Direct Torque Control of PMSM Drives," *IEEE Transactions on Energy Conversion,* pp. 1-10, 2023.

[14] Y. Luo, K. Yang, and Y. Zheng, "Feedback Linearization-Based Direct Torque Control for Asymmetrical Six-Phase PMSM Motor With Back EMF Harmonics Compensation," *IEEE Journal of Emerging and Selected Topics in Power Electronics,* vol. 11, pp. 5145-5155, 2023.

[15] O. E. Özçiflikçi, M. Koç, S. Bahçeci, and S. Emiroğlu, "Overview of PMSM control strategies in electric vehicles: a review," *International Journal of Dynamics and Control,* 2023/10/09 2023.

[16] O.E. Özçiflikçi., M. Koç "Comparison of interior mounted permanent magnet synchronous motor drives with sinusoidal, third harmonic injection, and space vector pulse width modulation strategies in particular attention to current distortions and torque ripples," *Electrica,* vol. 23, pp. 151-159, 2023.

[17] X. Wang, Z. Wang, M. Cheng and Y. Hu, "Remedial Strategies of T-NPC Three-Level Asymmetric Six-Phase PMSM Drives Based on SVM-DTC," in IEEE Transactions on Industrial Electronics, vol. 64, no. 9, pp. 6841-6853, Sept. 2017.

[18] H. Mesloub, R. Boumaaraf, M.T. Benchouia, A. Goléa, N. Goléa, K. Srairi," Comparative study of conventional DTC and DTC_SVM based control of PMSM motor — Simulation and experimental results" Mathematics and Computers in Simulation, vol.167, pp. 296-307, 2020.

[19] Q. Wang et al., "A Low-Complexity Optimal Switching Time-Modulated Model-Predictive Control for PMSM With Three-Level NPC Converter," in IEEE Transactions on Transportation Electrification, vol. 6, no. 3, pp. 1188-1198, Sept. 2020,

[20] Y. Wang, H. Li, R. Liu, L. Yang and X. Wang, "Modulated Model-Free Predictive Control With Minimum Switching Losses for PMSM Drive System," in IEEE Access, vol. 8, pp. 20942-20953, 2020

[21] M. Koç, "Unified Field Oriented Controlled Drive System for All Types of PMSMs Considering System Nonlinearities," *IEEE Access,* vol. 10, pp. 56773-56784, 2022.

[22] J. -S. Yim, S. -K. Sul, B. -H. Bae, N. R. Patel and S. Hiti, "Modified Current Control Schemes for High-Performance Permanent-Magnet AC Drives With Low Sampling to Operating Frequency Ratio," in IEEE Transactions on Industry Applications, vol. 45, no. 2, pp. 763-771, March-april 2009